Oviductal motile cilia are essential for oocyte pickup but dispensable for sperm and embryo transport

Shuiqiao Yuan[a,b,1], Zhuqing Wang[a,c], Hongying Peng[a], Sean M. Ward[a], Grant W. Hennig[a], Huili Zheng[a,c], and Wei Yan[a,c,d,1]

[a]Department of Physiology and Cell Biology, University of Nevada, Reno School of Medicine, Reno, NV 89557; [b]Institute of Reproductive Health, Tongji Medical College, Huazhong University of Science and Technology, Wuhan 430030, China; [c]Sections of Metabolic Diseases and Translational Genomics, The Lundquist Institute for Biomedical Innovation at Harbor–UCLA Medical Center, Torrance, CA 90502; and [d]Department of Medicine, David Geffen School of Medicine at UCLA, Los Angeles, CA 90095

Edited by Thomas E. Spencer, University of Missouri, Columbia, MO, and approved April 26, 2021 (received for review February 12, 2021)

Mammalian oviducts play an essential role in female fertility by picking up ovulated oocytes and transporting and nurturing gametes (sperm/oocytes) and early embryos. However, the relative contributions to these functions from various cell types within the oviduct remain controversial. The oviduct in mice deficient in two microRNA (miRNA) clusters (*miR-34b/c* and *miR-449*) lacks cilia, thus allowing us to define the physiological role of oviductal motile cilia. Here, we report that the infundibulum without functional motile cilia failed to pick up the ovulated oocytes. In the absence of functional motile cilia, sperm could still reach the ampulla region, and early embryos managed to migrate to the uterus, but the efficiency was reduced. Further transcriptomic analyses revealed that the five messenger ribonucleic acids (mRNAs) encoded by *miR-34b/c* and *miR-449* function to stabilize a large number of mRNAs involved in cilium organization and assembly and that *Tubb4b* was one of their target genes. Our data demonstrate that motile cilia in the infundibulum are essential for oocyte pickup and thus, female fertility, whereas motile cilia in other parts of the oviduct facilitate gamete and embryo transport but are not absolutely required for female fertility.

Fallopian tube | multiciliogenesis | ciliopathy | fertility | microRNAs

Oviducts, also called Fallopian tubes in humans, are a pair of tubular structures that connect the ovary to the uterus. The oviduct develops from the upper portion of the Müllerian/paramesonephric duct (1) and consists of four segments from the uterus to the ovary, including the uterotubal junction, isthmus, ampulla, and infundibulum. The oviduct consists of a smooth muscle wall lined with the epithelium containing mainly two cell types: ciliated cells and nonciliated secretory cells (also called "club" or Peg cells). Known functions of the oviduct include the following: 1) fimbriae of the infundibulum pick up the ovulated cumulus-oocyte complex (COC) (also called oocytes in cumulus) and transport the COC to the ampulla; 2) ampulla is the site where fertilization occurs; 3) the oviduct aids in transport of spermatozoa from the isthmus to the ampulla for fertilization; 4) the oviduct also transports fertilized eggs and preimplantation embryos from the ampulla, through the isthmus and uterotubal junction, eventually to the uterine cavity for implantation; and 5) the oviduct provides the optimal microenvironment via secretions and signaling that support survival and development of not only ovulated/fertilized eggs and preimplantation embryos but also spermatozoa (1). In summary, transport and nourishment appear to be the two major functions of the oviduct (1).

Secretory cells produce nutrients to support the viability of gametes (sperm and eggs) and early embryos, whereas transport is believed to be achieved through one, or a combination, of the following three factors: smooth muscle contraction, cilia beating, and flow of tubal fluid (2). The major mechanism underlying the transport function of the oviduct remains inconclusive. For example, two earlier reports showed that inhibition of smooth muscle contractility using isoproterenol in vitro did not compromise egg and embryo transport, suggesting smooth muscle contraction is not essential for the transport function (3, 4). However, some argue that this compound also increases cilia beating, which may have exaggerated the effects of cilia beating. Confusingly, the fact that mutant mice with ciliary dyskinesia and women with Kartagener's syndrome can still become pregnant (5–8) seems to support that smooth muscle contraction, not cilia beating, is responsible for transportation of the gametes and embryos. The relative contribution of smooth muscle contraction, cilia beating, and flow of secretion to the transport function of the oviduct remains debatable. We recently reported that global knockout (KO) of two miRNA gene clusters (*miR-34b/c* and *miR-449*) in mice leads to female infertility (9). The female infertility phenotype is likely caused by a lack of motile cilia in the oviductal epithelium because the KO females have normal hormonal profiles and normal folliculogenesis (9). The "cilia-less" oviducts in these KO female mice provided us with an unprecedented opportunity to define the physiological roles of motile cilia in the oviduct and also to reveal the molecular mechanism underlying normal development and function of ciliated cells in the oviduct. Here, we report that normal motile cilia are essential for the pickup of the ovulated oocytes by the infundibulum, and motile cilia in the isthmus and ampulla regions of the oviduct facilitate gamete and embryo transport but are not absolutely required for female fertility.

Significance

The oviduct is essential for female fertility due to its two main functions: transport and nourishment. While the nourishment role is mainly fulfilled by secretory cells, the relative contribution to the transport function by ciliated cells and smooth muscle cells remains controversial. Here, we show that functional motile cilia in the infundibulum are essential for oocyte pickup and transport, whereas motile cilia in the ampulla and isthmus regions of the oviduct facilitate gamete and embryo transport but are dispensable for female fertility. Knowledge derived from the present study may have important clinical implications in the areas including development of nonhormonal female contraceptives, understanding the cause of ectopic pregnancy and high-grade serous ovarian cancer, etc.

Author contributions: S.Y. and W.Y. designed research; S.Y., Z.W., H.P., S.M.W., G.W.H., and H.Z. performed research; S.Y., Z.W., H.P., S.M.W., G.W.H., H.Z., and W.Y. analyzed data; and S.Y. and W.Y. wrote the paper.

The authors declare no competing interest.

This article is a PNAS Direct Submission.

See online for related content such as Commentaries.

[1]To whom correspondence may be addressed. Email: shuiqiaoyuan@hust.edu.cn or wei.yan@lundquist.org.

This article contains supporting information online at https://www.pnas.org/lookup/suppl/doi:10.1073/pnas.2102940118/-/DCSupplemental.

Published May 26, 2021.

Results

miR-34b/c and miR-449a/b/c Are Abundantly Expressed in the Oviductal Epithelial Cells in Mice. To investigate the role of *miR-34b/c* and *miR-449* clusters in multiciliogenesis in the oviduct, we first analyzed expression levels of the five miRNAs encoded by the *miR-34b/c* and *miR-449* clusters in the wild-type (WT) oviducts using TaqMan-based miRNA quantitative real-time PCR (qPCR) analyses. All of the five miRNAs were detected in the WT (Fig. 1*A*) but undetectable in the global *miR-34b/c* and *miR-449* double KO (herein called miR-dKO) oviducts (Fig. 1*B*). To further determine the cell types that express these five miRNAs, we prepared the enriched epithelial and smooth muscle cell fractions, and the purity of each fraction was monitored by qPCR analyses of marker genes for the oviductal epithelium (*Ovgp1* and *Krt8*) and smooth muscle (*Des* and *Acta2*) (Fig. 1*C*). Using the highly enriched oviductal epithelial and smooth muscle cells, we further examined the levels of the five miRNAs in WT and miR-dKO oviducts (Fig. 1*A*). All of the five miRNAs were predominantly expressed in WT, but not in miR-dKO, oviductal epithelial cells (Fig. 1 *A* and *D*). Detection of trace amounts of the five miRNAs in the smooth muscle cells was likely due to contaminations by the epithelial cells (Fig. 1 *A* and *C*). Taken together, the five miRNAs encoded by the two miRNA clusters are predominantly expressed in the oviductal epithelial cells.

miR-34b/c and miR-449a/b/c Are Essential for Oviductal Multiciliogenesis during Development. To characterize the oviductal phenotype in the miR-dKO female mice, we examined the morphology of WT and miR-dKO oviducts (Fig. 2 *A–D*). The miR-dKO oviducts appeared to be less coiled and thus, shorter, as compared to the WT oviducts (Fig. 2 *A* and *C*). The ampulla region of the miR-dKO oviducts was less prominent than that in the WT controls (Fig. 2 *A* and *C*). Consistent with gross morphology, histology of the miR-dKO oviducts showed fewer infoldings and atrophic epithelium (Fig. 2*D*) compared to the WT controls (Fig. 2*B*). While abundant in the WT oviductal epithelium (Fig. 2 *B*, *Lower*), cilia were hardly seen in the epithelium of miR-dKO oviducts (Fig. 2 *D*, *Lower*). Transmission electron microscopy (TEM) revealed abundant, apically pointed cilia anchored to well-aligned basal bodies in the WT oviducts (Fig. 2*E*). In contrast, the basal bodies were sporadically seen but mostly misaligned, and only apically docked basal bodies were associated with shorter cilia in the miR-dKO oviducts (Fig. 2*E* and *SI Appendix*, Fig. S1). However, the typical "9+2" microtubes of the axoneme were not affected in the miR-dKO oviducts (Fig. 2*F*). Further imaging analyses of the whole-mount oviducts revealed vigorous beating of motile cilia in the WT oviducts (Movie S1), whereas the cilia beating was much weaker, and the cilia appeared to be much shorter in the miR-dKO oviducts (Movie S2). Imaging analyses of single-cell preparations of the oviductal epithelium verified the observations from the whole-mount analyses, showing strong cilia beating of ciliated cells in WT (Movie S3) but no or much weaker cilia movements in ciliated cells in the miR-dKO oviducts (Movie S4).

Isolated ciliated cells from the WT oviduct epithelium displayed bulbous circular or ovoid cell bodies with a ciliated fringe occupying a quadrant of the cell surface (*SI Appendix*, Fig. S2*A*). The cilia were, on average, 5.1 ± 0.6_{sd} μm in length (n = 6) and moved back and forth by ∼30° (*SI Appendix*, Fig. S2*A*). The movement of cilia was not uniform throughout the fringe, and typically three to five regions in the fringe had their own rhythms that moved in and out of phase with adjacent regions over time (*SI Appendix*, Fig. S2 *A* and *B*). In intact segments of isolated infundibulum of WT oviducts, the inner lining showed strong rhythmic cilia movements at a frequency of ∼6 Hz (*SI Appendix*, Fig. S2 *C* and *D*). The vigorous motions were detected as large changes in the translucency of the lining due to the clumping and separation of cilia over time. Slow moving waves (see white streaks in *SI Appendix*, Fig. S2*D*) emerged within the ongoing rhythmic movement and appeared to propagate long distances along the epithelial lining (>100 μm). The pattern of cilia movement in the intact segments of isolated miR-dKO infundibulum was noticeably different. Regions of the epithelium

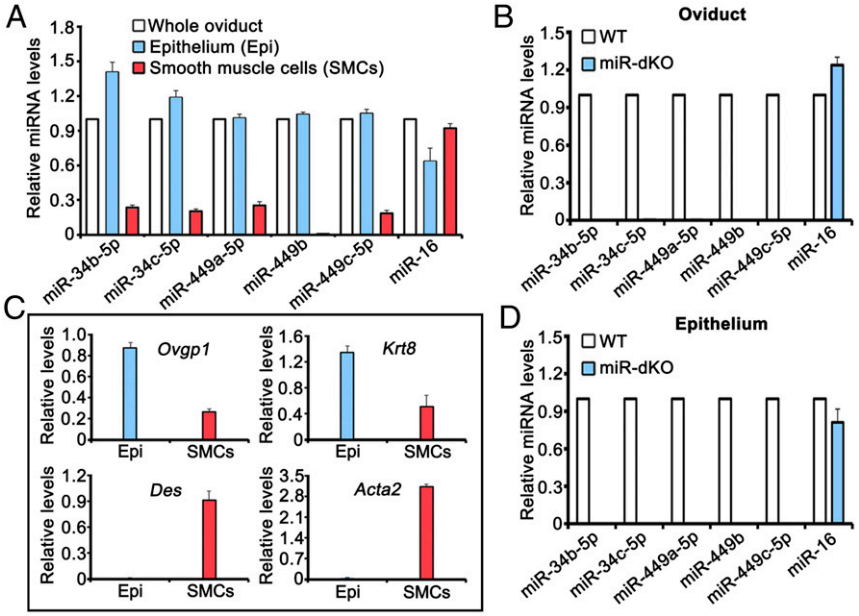

Fig. 1. Five miRNAs encoded by the *miR-34b/c* and *miR-449* clusters are preferentially expressed in the epithelial cells of the oviducts. (*A*) qPCR analyses of the five miRNAs (miR-34b/c and miR-449a/b/c) in the total oviduct, oviductal epithelial, and smooth muscle cells purified from WT female mice. miR-16 was included as a positive control. (*B*) qPCR analyses of the five miRNAs (miR-34b/c and miR-449a/b/c) in WT and miR-dKO oviducts. miR-16 was included as a positive control. (*C*) qPCR analyses of levels of oviductal marker genes, including *Ovgp1* and *Krt8* (oviductal epithelial cell markers) and *Des* and *Acta2* (smooth muscle cell makers), in enriched epithelial and smooth muscle cells from WT oviducts. (*D*) qPCR analyses of the five miRNAs (miR-34b/c and miR-449a/b/c) in WT and miR-dKO oviductal epithelial cells. miR-16 was included as a positive control. All qPCR assays were performed in biological triplicates, and the data were presented as mean ± SEM.

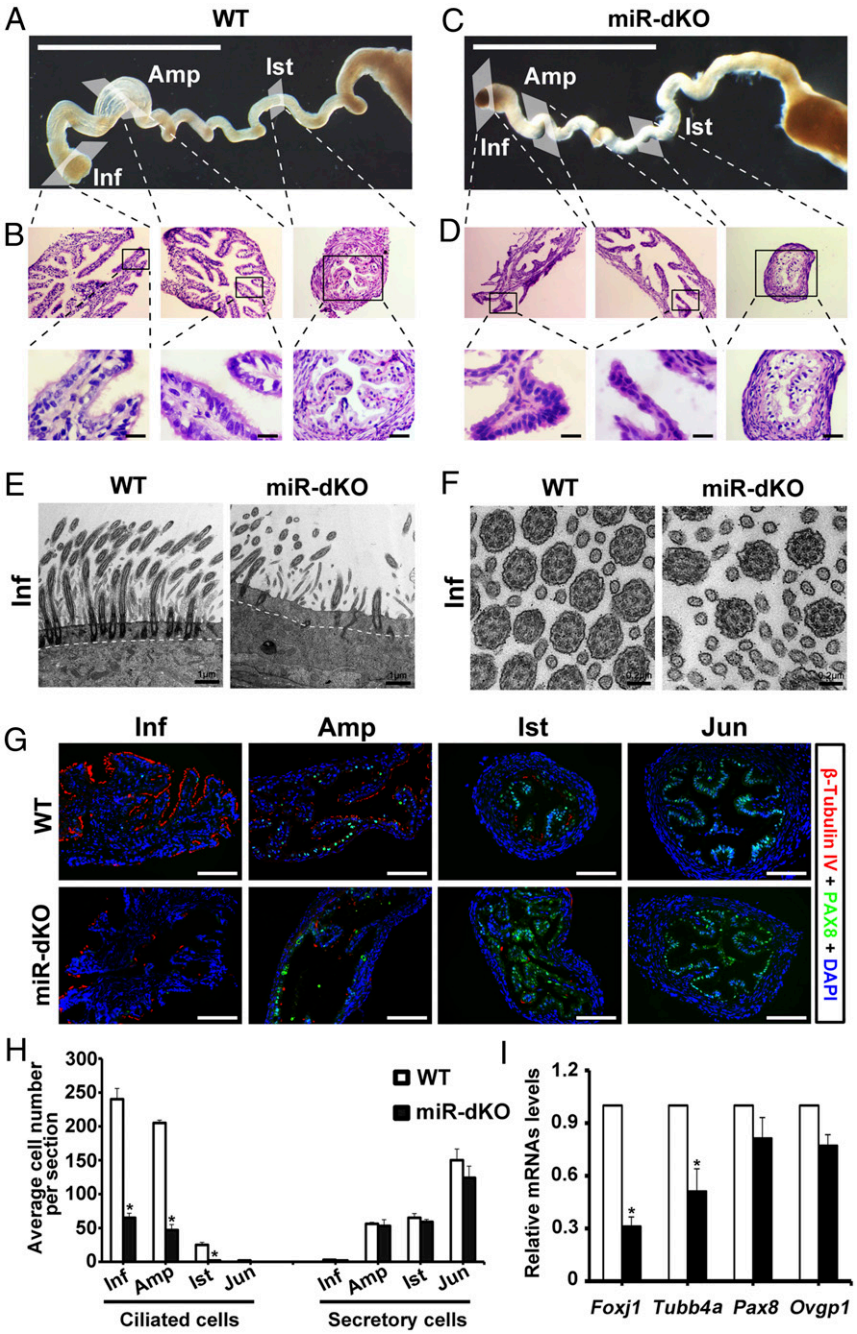

Fig. 2. Ablation of *miR-34b/c* and *miR-449* disrupts multiciliogenesis in the oviductal epithelium. (*A*) Gross morphology of WT oviducts. (Scale bar, 1 mm.) (*B*) Low-power images showing histology of the WT oviductal infundibulum (Inf), ampulla (Amp), and isthmus (Ist) from the boxed areas in *A* (*Upper*). *Lower* are higher magnifications of the boxed areas from *Upper*, showing the presence of motile cilia pointing to the lumen. (Scale bar, 10 μm.) (*C*) Gross morphology of miR-dKO oviducts. (Scale bar, 1 mm.) (*D*) Low-power images showing histology of the miR-dKO oviductal infundibulum (Inf), ampulla (Amp), and isthmus (Ist) from the boxed areas in *C* (*Upper*). *Lower* are higher magnifications of the boxed areas from *Upper*, showing the absence of motile cilia. (Scale bar, 10 μm.) (*E* and *F*) Ultra-structure of the ciliated epithelium in WT and miR-dKO oviducts revealed by TEM. The miR-dKO epithelium contains much fewer cilia with fewer and misaligned basal bodies, as compared to WT control (*E*). However, the typical ciliary "9+2" microtubules are present in both WT and miR-dKO controls (*F*). Scale bars are marked on the images. Five WT and miR-dKO mice were analyzed, and representative images are shown. (*G*) Representative immunofluorescence images showing β-tubulin IV–positive (ciliated) and PAX8-positive (secretory) cells in infundibulum (Inf), ampulla (Amp), and isthmus (Ist) of the WT and miR-dKO oviducts. (Scale bar, 100 μm.) (*H*) Quantification of ciliated and secretory cells in Inf, Amp, Ist, and uterotubal junction of WT and miR-dKO oviducts based on immunofluorescent labeling. Data are presented as mean ± SEM ($n = 3$), $^*P < 0.05$. (*I*) qPCR analyses of marker genes for ciliated (*Foxj1* and *Tubb4a*) and secretory (*Pax8* and *Ovgp1*) cells in WT and miR-dKO oviducts. Data are presented as mean ± SEM ($n = 3$), $^*P < 0.05$.

showing movement were patchy (*SI Appendix*, Fig. S2*E*), and the oscillations in those regions were weaker and occurred at a high frequency (12 Hz instead of 6 Hz) (*SI Appendix*, Fig. S2*F*). Since the five miRNAs encoded by the two miRNA clusters are absent since fertilization, the defects in the adult global miR-dKO oviducts are likely reflecting an essential role of these five miRNAs in initial multiciliogenesis in the oviductal epithelium during development.

miR-34b/c and miR-449a/b/c Are Also Required for Multiciliogenesis in Adult Oviductal Epithelia. To further confirm that the ciliary defects are truly caused by a loss of function of *miR-34b/c* and *miR-449* clusters, we crossed the *Foxj1*-Cre mouse line, which expresses Cre recombinase exclusively in ciliated cells of the oviductal epithelium (10), with *miR-34b/c*$^{-/-}$*miR-449*$^{loxp/loxp}$ mice to generate conditional KO mice with *miR-34b/c* and *miR-449* specifically inactivated in the ciliated cells of the oviductal epithelium (termed Foxj1-Cre-miR-dKO). The fecundity tests reveal that ∼57% (8 out of 14) of Foxj1-Cre-miR-dKO females were completely infertile (*SI Appendix*, Fig. S3*A*). Although the remaining ∼43% (6 out of 14) Foxj1-Cre-miR-dKO females were initially fertile, both their litter size and litter interval were greatly reduced compared to WT controls (*SI Appendix*, Fig. S3 *B* and *C*), and their fertility progressively decreased with age and became completely infertile after 6 mo of age. Histological analyses further revealed that multiciliogenesis is defective in the Foxj1-Cre-miR-dKO oviducts, similar to that in the global miR-dKO oviducts (*SI Appendix*, Fig. S4). Of interest, the completely infertile Foxj1-Cre-miR-dKO females all showed a complete loss of cilia in the oviducts, whereas those with initial fertility always contained some cilia, especially in the infundibulum of the oviducts (*SI Appendix*, Fig. S4). Consistently, immunostaining with acetylated-α-tubulin (Ac-α-tub, a marker for motile cilia) showed that the number of cilia was greatly decreased in the infundibulum, ampulla, and isthmus of the Foxj1-Cre-miR-dKO oviducts compared to WT controls (*SI Appendix*, Fig. S5). The data suggest that fertility in the Foxj1-Cre-miR-dKO females correlates positively with the abundance of motile cilia in the oviductal epithelium; that is, the more cilia, the more fertile. A similar phenotype observed between the global and conditional KO mice strongly suggests that ablation of the miRNA clusters indeed causes defects in oviductal multiciliogenesis.

The incomplete penetrance of the oviductal phenotype may result from a late onset of Cre activity in the Foxj1-Cre-miR-dKO oviducts. To test this possibility, we crossed the Foxj1-Cre with mTmG reporter mice and observed that Foxj1-Cre was turned on, as indicated by membrane-tagged green fluorescence (mG) expression, in the oviductal epithelium at ∼postnatal day 4 (P4) (*SI Appendix*, Fig. S6). This means that the two miRNA clusters started to be inactivated at ∼P4. Given that multiciliogenesis in the oviductal epithelium starts at ∼P4 (11), such a late onset of inactivation of the two miRNA clusters would allow for initiation and even completion of the first wave of multiciliogenesis in the Foxj1-Cre-miR-dKO oviductal epithelium, which may explain why ∼43% of the Foxj1-Cre-miR-dKO females were initially fertile. The fact that these conditional KO females gradually lost their fertility due to completely failed multiciliogenesis suggests that the five miRNAs are required for oviductal multiciliogenesis during adulthood. In the completely infertile Foxj1-Cre-miR-dKO females, which accounted for 57% of the total conditional KO females, their oviducts were more similar to the global KO females with atrophic appearance, whereas those that were initially fertile and later became infertile had oviducts more like the WT. The morphological defects observed in both global and conditional KO oviducts suggest that inactivation of the two miRNA clusters will cause atrophic oviductal epithelia no matter when the inactivation occurs (during development versus adulthood). Therefore, it is highly likely that both the atrophic epithelium and lack of cilia may have contributed to the failure in COC pickup. Together, the five miRNAs are essential for not only initial multiciliogenesis in the oviductal epithelium during development but also for normal homeostasis of the oviductal epithelium in adulthood.

miR-34b/c and miR-449a/b/c Are Dispensable for Secretory Cell Development in the Oviductal Epithelium. The oviductal epithelium in adult female mice consists of two major cell types: ciliated and secretory cells. To determine whether secretory cells are also implicated in the epithelium of the miR-dKO oviducts, we performed coimmunofluorescent staining of β-tubulin IV (a ciliated cell marker) and PAX8 (a secretory cell marker) to visualize ciliated and secretory cells in the oviductal epithelium (Fig. 2*G*). In WT oviducts, β-tubulin IV–positive cells were detected in the epithelium of infundibulum, ampulla, and isthmus (Fig. 2 *G*, *Upper*), and the number of ciliated cells (β tubulin IV positive) gradually decreased from infundibulum to isthmus (Fig. 2*H*). On the contrary, the PAX8-positive cells were dominant in the epithelium of ampulla, isthmus, and junction site (Fig. 2 *G*, *Upper*), and the number of secretory cells (PAX8 positive) increased from ampulla to isthmus and uterotubal junction. In contrast, in the epithelium of miR-dKO oviducts, β-tubulin IV–positive cells were much fewer (Fig. 2 *G*, *Lower*), and the number of ciliated cells was significantly reduced, as compared to WT oviductal epithelium (Fig. 2*H*). No significant differences were noted in either the number or the density of the PAX8-positive secretory cells along the four segments of the WT and miR-dKO oviducts (Fig. 2*H*). Consistently, qPCR analyses revealed that levels of *Foxj1* and *Tubb4a*, two marker genes for ciliated cells, were significantly down-regulated, but levels of *Pax8* and *Ovgp1* (secretory cell marker gene) remained largely unchanged in miR-dKO oviducts, as compared to WT controls (Fig. 2*I*). Given that inactivation of the two miRNA clusters leads to a reduced number of ciliated cells and a lack of cilia on most of the ciliated cells (Fig. 2 *G–I*), it is not surprising that the KO oviducts are somewhat atrophic compared to WT controls (Fig. 2 *A–D*). These data indicate that loss of the two miRNA clusters affects mainly the ciliated cells but not the secretory cells in the oviductal epithelium.

Functional Motile Cilia in Infundibulum Are Essential for Picking up the Ovulated Oocytes. We have previously shown that folliculogenesis in the miR-dKO females is largely normal, but no metaphase II (MII) oocytes can be retrieved from the oviducts despite the production of germinal vesicle (GV) oocytes with normal quantity and quality (9). These findings strongly suggest that the infundibulum in the miR-dKO oviducts may not be able to pick up the ovulated COCs. If this is the case, the ovulated COCs should, in theory, be trapped inside the ovarian bursa cavity in the miR-dKO female mice (Fig. 3*A*). To prove this, we carefully dissected out the entire ovarian bursa together with the ovary and the infundibulum that it enveloped (Fig. 3*B*). Following fixation and dehydration, the entire structure was embedded into paraffin for histological analyses. By sectioning through the entire paraffin blocks followed by hematoxylin-eosin staining, we detected ovulated COCs in the ampulla of the WT oviducts (Fig. 3 *C* and *D*), but no COCs were present in the ampulla of the miR-dKO oviducts; instead, the ovulated COCs were found inside the ovarian bursa cavity (Fig. 3 *E–H*). The fact that COCs are trapped inside the ovarian bursa suggests that the ovulated COCs fail to be picked up by fimbriae of the infundibulum, explaining why COCs are absent in the ampulla of the oviduct in miR-dKO females. Given that the major structural difference between WT and miR-dKO oviducts lies in the lack of cilia, our data strongly suggest that motile cilia in the infundibulum are essential for COC pickup.

Motile Cilia Facilitate, but Are Dispensable for, Sperm and Embryo Transport. Oviductal transport of sperm and preimplantation embryos is believed to be achieved through combined effects of cilia beating, muscular contraction, and tubal fluid flow (12). However, the relative contribution from these three factors remains controversial (3, 4, 13, 14). The miR-dKO female mice have fewer ciliated cells largely devoid of motile cilia, while other cell types, including secretory cells and smooth muscle cells, appear to be histologically normal (Figs. 1 and 2), thus representing a good model to assess the relative contribution of motile cilia beating versus smooth muscle contraction to the sperm and embryo transport function. To monitor sperm migration through the oviduct, we

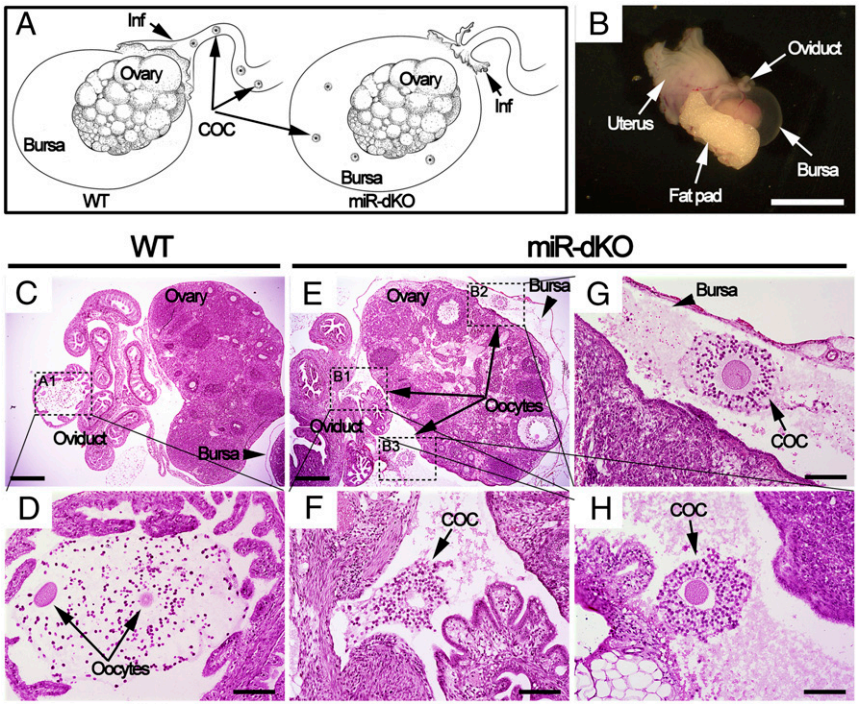

Fig. 3. Ovulated oocytes are trapped inside the ovarian bursa cavity in miR-dKO female mice, as revealed by whole-mount histology analyses. (*A*) Schematics showing our hypothesis; that is, the ovulated COCs are picked up by fimbriae of the infundibulum and further transported to ampulla for fertilization in WT oviducts (*Left*), whereas the ovulated COCs fail to be picked up by fimbriae of the infundibulum in miR-dKO female mice and consequently fall into the ovarian bursa cavity (*Right*). (*B*) Gross morphology of the female reproductive system ~3 h after ovulation, including the oviduct, bursa, ovary, fat pad, and uterus. (Scale bar, 5 mm.) (*C*) A cross-section showing histology of the ovary, oviducts, and bursa. (Scale bar, 0.5 mm.) (*D*) Digital enlargement of the ampulla region of the oviduct (framed in *C*), where two oocytes (arrows) are present. (Scale bar, 0.1 mm.) (*E*) A cross-section showing that the ovulated oocytes are trapped inside the bursa cavity in miR-dKO mice. (Scale bar, 0.5 mm.) (*F–H*) Digital magnification of three areas (framed in *E*), where individual COCs are present inside the bursa. (Scale bar, 0.1 mm.) Both WT and miR-dKO mice in this experiment were primed with pregnant mare's serum gonadotropin and hCG, and the samples were collected 15 h after hCG injection. COC, cumulus-oocyte complex; Inf, infundibulum. $n = 4$ for each genotype.

used *Stra8-Cre-mTmG*$^{+/Tg}$ male mice because their sperm are green under a fluorescent microscope due to expression of the mG (*SI Appendix*, Fig. S7). The whole-mount oviducts are translucent, thus allowing for direct observation of the green sperm under the fluorescent microscope. The whole oviducts were dissected from WT (Fig. 4*A*) and miR-dKO (Fig. 4*B*) female mice ~3 h postcopulation. Large bundles of "green" sperm were observed in both the ampulla and isthmus regions of the WT oviducts (Fig. 4 *C* and *D*). In contrast, much fewer sperm were observed at similar locations in the miR-dKO oviducts (Fig. 4 *E* and *F*). By flushing out all of the sperm from the oviducts, we determined that the total sperm counts were much less in the miR-dKO than in the WT oviducts (Fig. 4*G*). Of note, while the oocytes were clearly visible in the ampulla of the WT oviducts, no oocytes were seen in the "ampulla-like" region of the miR-dKO oviducts (Fig. 4 *A* and *B*). This is consistent with the finding that the oocytes were trapped inside the ovarian bursa cavity in the miR-dKO females (Fig. 3). The fact that sperm transport, despite reduced efficiency, still occurs in the absence of motile cilia suggests that normal motile cilia in the oviductal epithelium facilitate sperm transport, but it is not absolutely required.

Next, we tested whether motile cilia in the oviductal epithelium are required for the transport and normal development of the preimplantation embryos. We transferred two-cell embryos into the oviducts (Fig. 4*H*) and blastocysts to the uterus (Fig. 4*I*) of WT and miR-dKO recipient female mice. Interestingly, all of the recipient miR-dKO female mice, including four for oviductal transfer and three for uterine transfer, became pregnant, reached full term, and delivered pups (Fig. 4*J*). No significant differences in birth rate were observed between WT and miR-dKO groups when uterus transfer was performed (Fig. 4*J*). However, the rate of live-born pups was significantly reduced in the miR-dKO oviduct transfer group than in the WT control group (Fig. 4*J*). These data indicate that the "cilia-less" miR-dKO oviducts are able to support transport and development of early embryos. Therefore, motile cilia in the oviductal epithelium facilitate the transport and development of preimplantation embryos but are not absolutely essential.

Loss of miR-34b/c and miR-449a/b/c Does Not Compromise the Oviductal Pacemaker Activity. To assess whether the electrical pacemaker activity underlying myosalpinx phasic muscular contractility is impaired in the oviduct of miR-dKO females, we performed intracellular electrical recordings using dissected oviducts in vitro, as reported previously (14). The membrane potential and spontaneous pacemaker activity termed electrical slow waves were recorded from both WT and miR-dKO oviducts, and the data are presented as both individual representative traces (Fig. 5 *A–D*) and the summarized slow wave parameters (Fig. 5 *E–L*). Resting membrane potential (RMP) from the ampulla and isthmus regions of WT controls averaged −58.2 ± 1.0 mV and −57.5 ± 1.5, respectively ($n = 6$ WT oviducts). Rhythmic slow waves from the ampulla and isthmus regions of WT controls averaged 32.5 ± 2.0 mV and 31.6 ± 1.8 mV in amplitude and 2.2 ± 0.4 and 2.8 ± 0.6 s in duration and occurred at a frequency of 9.8 ± 1.5 and 9.2 ± 1.2 cycles min^{-1}, respectively (Fig. 5 *A* and *B*). There was no statistical difference in slow wave parameters between the ampulla and isthmus regions in WT controls ($P = 0.45$, $P = 0.2$, and $P = 0.38$, respectively; $n = 6$ WT oviducts) (Fig. 5 *E–L*). In the ampulla and isthmus regions of miR-dKO oviducts, RMP averaged 57.0 ± 2.8 mV and −56.0 ± 3.0

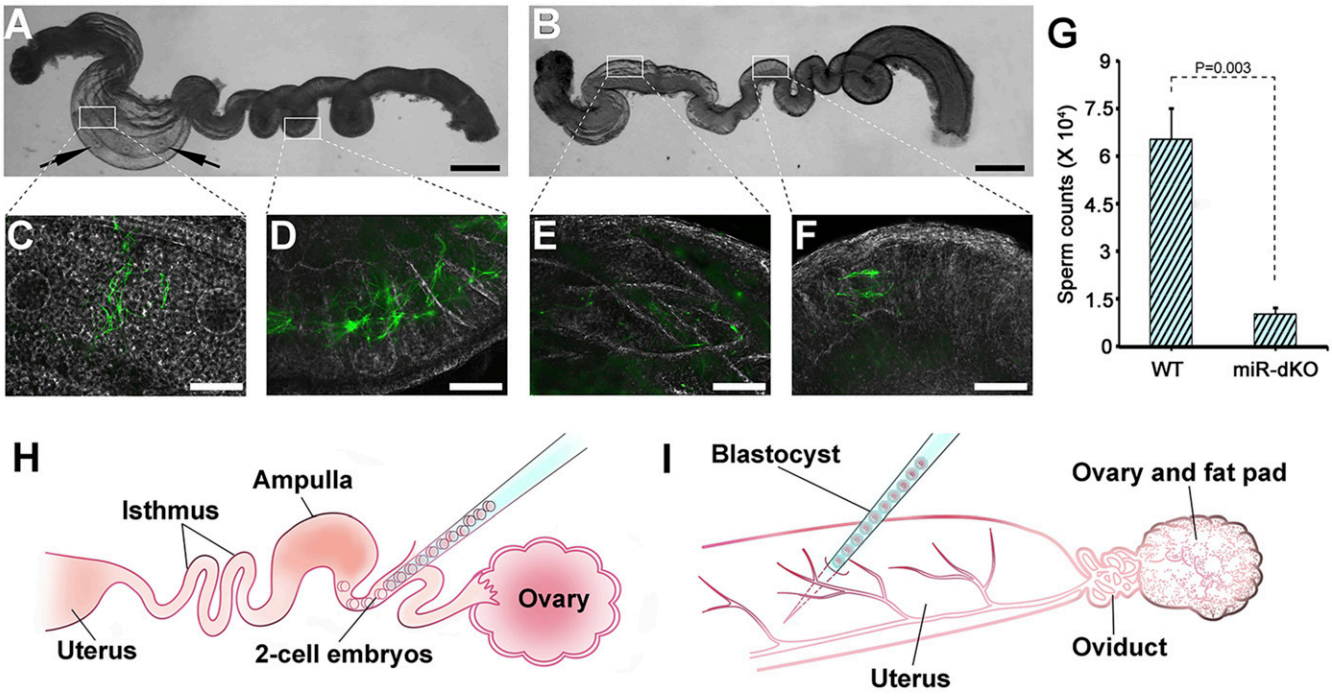

J

Transfer position	Genotype of recipients	No. of recipients	Stage of transferred WT embryos (n)	Terms of pregnancy	No. (%) of live pups delivered
Oviduct	WT	3	2-cell (51)	+,+,+	20 (39.2)
	dKO	4	2-cell (72)	+,+,+,+	14 (19.4)*
Uterus	WT	3	Blastocyst (30)	+,+,+	16 (53.3)
	dKO	3	Blastocyst (30)	+,+,+	11 (36.6)

*$P<0.05$, χ^2 test, compared to WT group.

Fig. 4. The sperm and embryo transport function is compromised in the miR-dKO oviducts. (*A* and *B*) Whole oviducts dissected from pregnant mare's serum gonadotropin/hCG-primed WT (*A*) and miR-dKO (*B*) females mated with *Stra8-Cre-mTmG*$^{+/Tg}$ males. Arrows indicate the presence of oocytes within the oviductal ampulla. (Scale bar, 1 mm.) (*C* and *D*) High-power images under transillumination of the two boxed areas in *A,* showing green sperm inside the oviductal ampulla and isthmus of WT females. (Scale bar, 100 μm.) (*E* and *F*) High-power images under transillumination of the two boxed areas in *B*, showing green sperm inside the oviductal ampulla and isthmus of miR-dKO females. (Scale bar, 100 μm.) (*G*) Qualification of sperm counts within the oviducts of WT and miR-dKO females ~3 h after mating with *Stra8-Cre-mTmG*$^{+/Tg}$ males. Data are presented as mean ± SEM ($n = 3$). (*H* and *I*) Schematics showing transfer of two-cell embryos into WT and miR-dKO oviduct (*H*), and transfer of blastocyst into WT and miR-dKO uterus (*I*). (*J*) Summary of the full-term development of WT embryos transferred into WT and miR-dKO oviducts or uteri.

mV, respectively ($n = 4$ miR-dKO oviducts). Rhythmic slow waves averaging 30.3 ± 5.0 and 29.8 ± 2.0 mV in amplitude and 3.2 ± 0.6 and 3.5 ± 2.1 s in duration occurred at a frequency of 11.1 ± 2.1 s and 9.8 ± 2.8 s for ampulla and isthmus of the miR-dKO oviducts, respectively (Fig. 5 *C* and *D*). Despite the seemingly irregularity in the slow waves recorded from some of the miR-dKO oviducts, there were no statistical differences either between the two regions of the miR-dKO oviducts or between miR-dKO and WT female mice ($P = 0.4$, $P = 0.36$, and $P = 0.32$, respectively; $n = 4$ miR-dKO oviducts) (Fig. 5 *E–L*). Associated with each slow wave was a phasic contraction of the myosalpinx in that region of the oviduct, which was observed through the microscope eyepieces, as reported previously (14). These data demonstrate that the pacemaker activity persisted in the myosalpinx of miR-dKO oviducts and smooth muscle contraction was not significantly impaired in the miR-dKO oviducts.

***Tubb4b* Is a Target Gene of miR-34b/c and miR-449a/b/c and Involved in Multiciliogenesis in the Oviductal Epithelium.** To gain molecular insights, we performed RNA sequencing (RNA-seq) using enriched oviductal epithelial and smooth muscle cells from WT and miR-dKO females (*SI Appendix*, Fig. S8). The RNA-seq analyses revealed that a total of 600 mRNAs were significantly dysregulated in the epithelial cells of the miR-dKO oviducts, whereas only 52 differentially expressed mRNAs were detected in smooth muscle cells of the miR-dKO oviducts ($P < 0.05$, fold change >2) (Fig. 6*A* and *SI Appendix*, Tables S1 and S2). Interestingly, among the 600 dysregulated mRNAs detected in the epithelial cells of miR-dKO oviducts, 598 were down-regulated, while only two were up-regulated (Fig. 6*A* and *SI Appendix*, Fig. S9), suggesting that the major function of miR-34b/c and miR-449a/b/c in vivo is to stabilize these mRNAs in the oviductal epithelium. Gene ontology term analyses revealed that these dysregulated, oviductal epithelial genes were mostly enriched for cilium assembly, cilium organization, and protein stabilization (Fig. 6*B*), which are supportive of the phenotype observed in miR-dKO oviducts, that is, defects in oviductal multiciliogenesis. Further in silico miRNA target prediction analyses using the 600 dysregulated mRNAs in the epithelial cells of the miR-dKO oviducts identified 24 potential targets of the five miRNAs encoded by the two miRNA clusters (*SI Appendix*, Table S3). In addition,

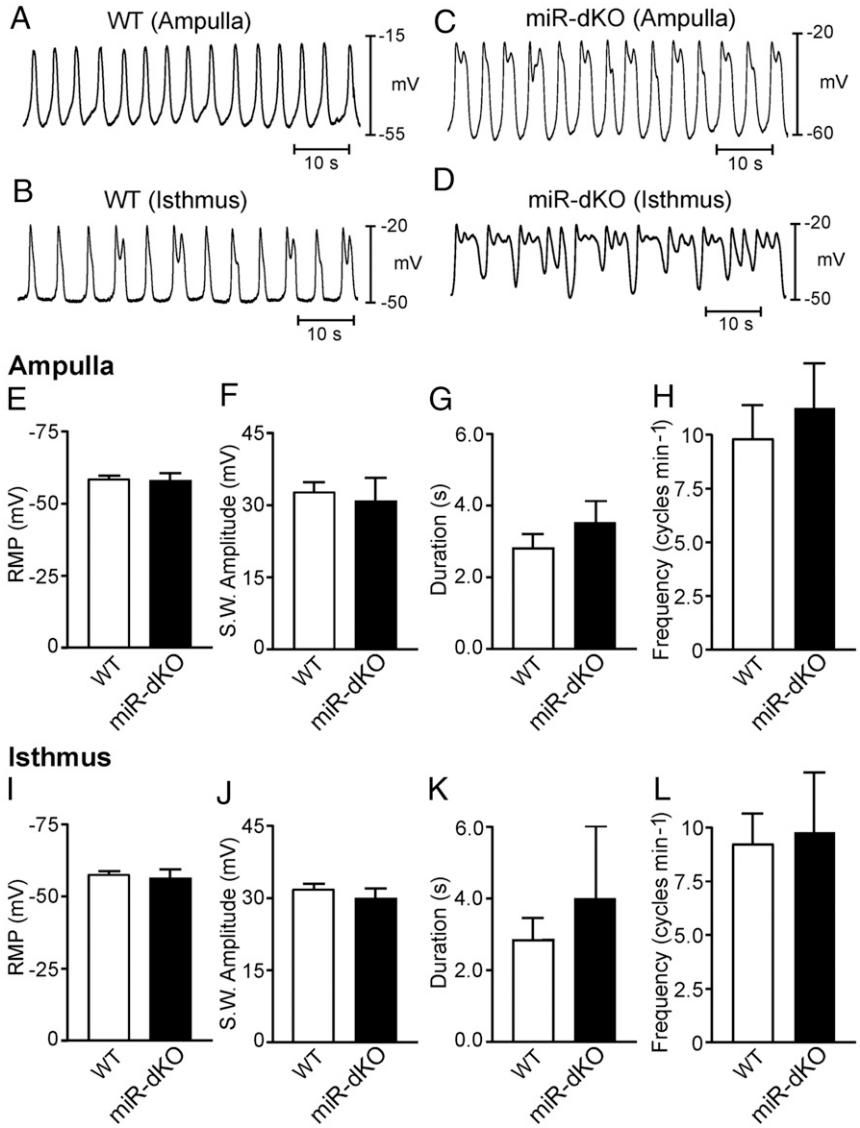

Fig. 5. Intracellular microelectrode recordings reveal that pacemaker activity in the myosalpinx is comparable between WT and miR-dKO oviducts. (*A* and *B*) Representative traces showing spontaneous pacemaker activity termed electrical slow waves recorded from the ampulla (*A*) and isthmus (*B*) regions of WT oviducts. (*C* and *D*) Representative traces showing slow waves recorded from the ampulla (*C*) and isthmus (*D*) regions of miR-dKO oviducts. (*E–H*) Summarized RMP (mV) (*E*) and slow wave parameters including amplitude (mV) (*F*), duration (*G*), and frequency (cycles min^{-1}) (*H*) in the ampulla region of WT (white bars; $n = 6$) and miR-dKO (black bars; $n = 4$) oviducts. (*I–L*) Summarized RMP (mV) (*I*) and slow wave parameters including amplitude (mV) (*J*), duration (*K*), and frequency (cycles min^{-1}) (*L*) in the isthmus region of WT (white bars; $n = 6$) and miR-dKO (black bars; $n = 4$) oviducts. No statistical differences in membrane potential or slow wave electrical parameters in either ampulla or isthmus regions between WT and miR-dKO oviducts.

down-regulation of the potential targets of miR-34b/c and miR-449a/b/c was further validated using qPCR analyses (Fig. 6*C*). *Tubb4b* was chosen for validation using the luciferase-based reporter assays because it has also been identified as a target of the five miRNAs in the efferent ducts (15). Indeed, the relative luciferase activity was significantly enhanced in the presence of miR-34b, miR-34c, miR-449a, and miR-449b, as compared to the negative control (NC) (Fig. 6 *D* and *E*), indicating that miR-34b/c and miR-449a/b truly target *Tubb4b* to stabilize its transcripts. Taken together, these data suggest that the five miRNAs play a pivotal role during multiciliogenesis in the oviductal epithelium by stabilizing dozens of their target mRNAs (Fig. 6*F*).

Discussion

We and others have previously reported that five miRNAs encoded by the *miR-34b/c* and *miR-449* clusters function to control multiciliogenesis in four organs containing motile cilia, including brain, trachea, efferent ducts, and oviducts (9, 16). The identical phenotype in the efferent ducts of global (*miR-34b/c*$^{-/-}$; *miR-449*$^{-/-}$) and ciliated cell-specific (*Foxj1-Cre; miR34b/c*$^{-/-}$; *miR449*$^{lox/del}$) KO males (15) suggests that the disrupted multiciliogenesis in the efferent ducts of the global KO males is indeed caused by the absence of the five miRNAs. Similarly, data reported here, including abundant expression of the five miRNAs in the oviductal epithelium and similar disruptions in oviductal multiciliogenesis between the global and conditional KO females, support the notion that the physiological role of the five miRNAs in the female reproductive system is to control multiciliogenesis in the oviductal epithelium.

The miR-dKO females are completely infertile despite normal folliculogenesis and ovulation (9). The fact that no COCs have ever been retrieved from the ampulla of the oviducts and that the

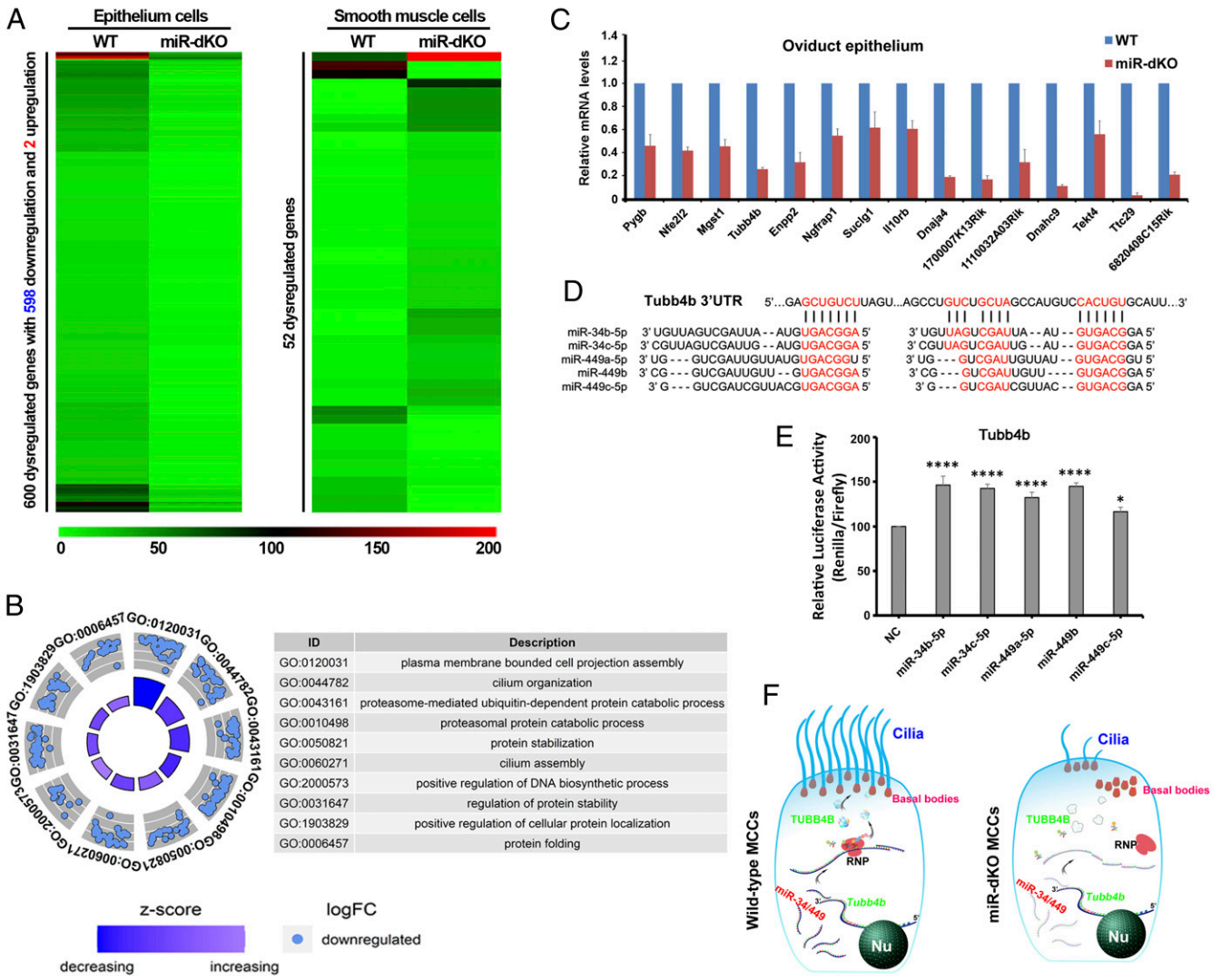

Fig. 6. RNA-seq analyses reveal that the five miRNAs encoded by the *miR-34b/c* and *miR-449* clusters control multiciliogenesis by stabilizing their targeted genes in the oviductal epithelium. (*A*) Heatmap showing significantly dysregulated mRNAs in the oviductal epithelial cells (*Left*) and smooth muscle cells (*Right*) of miR-dKO females, as compared to that of WT controls. A total of 600 and 52 dysregulated genes were identified in epithelial cells and smooth muscle cells of miR-dKO oviducts, respectively. (*B*) Circle plots showing the top 10 Gene Ontology (GO) terms analyzed from 598 down-regulated genes in miR-dKO oviductal epithelial cells. (*C*) qPCR validation of target gene expression levels in the oviductal epithelium of WT and miR-dKO females. *Gapdh* was used as an internal control. Data are presented as mean ± SEM ($n = 3$). (*D*) A schematic representation showing the two predicted miR-34/449 binding sites in the 3′ UTR of *Tubb4b* mRNA in mice. (*E*) Results of luciferase-based reporter assays showing that four out of the five miRNAs (miR-34b/c and miR-449a/b) could stabilize *Tubb4b* expression. Data are presented as mean ± SEM ($n = 3$). One-way ANOVA and Bonferroni correction were used for the multiple comparisons. ****$P < 0.0001$; *$P < 0.05$. (*F*) Schematics showing that miR-34b/c and miR-449 clusters regulate multiciliogenesis in oviductal epithelium by stabilizing numerous target genes involved in multiciliogenesis (e.g., *Tubb4b*). Nu, nucleus; RNP, ribonucleoprotein.

miR-dKO oviducts are mostly "cilia-less" strongly suggests that the infundibulum without functional motile cilia fails to pick up the ovulated COCs. Indeed, unlike WT mice with ovulated COCs located in the ampulla of the oviducts, the ovulated COCs are trapped within the ovarian bursa cavity in miR-dKO mice. This finding unequivocally demonstrates that the true reason for the infertility phenotype of miR-dKO female mice lies in the failure of the infundibulum to pick up the ovulated COCs during ovulation. Both previous reports and our data here show that the infundibulum of the oviducts contains the highest density of ciliated cells (11). The highest number of ciliated cells in the infundibulum is consistent with an essential role of motile cilia in COC pickup.

COCs are ovulated into the ovarian bursa cavity in rodents and into the peritoneal cavity of humans (17, 18). COC pickup by the oviductal infundibulum is a complex process involving both ciliary beating and adhesion between the oviductal epithelium and the COCs (19, 20). Adhesive interactions between the matrix of the COCs and ciliary crowns of the oviduct ensure that COCs stick well to the oviductal epithelium while motile cilia beating moves COCs over the surface of the infundibulum and into the ostium of the oviduct. Disruptions of the COC matrix abolishes COC pickup, suggesting an essential role of the COC matrix in COC pickup (18). Although changes in ciliary beating frequency have been shown to affect COC pickup rate, an essential role of cilia beating in the adhesion of COCs to oviductal epithelium has not been demonstrated. Here, we show that a lack of cilia, similar to the dysfunctional COC matrix, can also abolish COC pickup, suggesting that motile cilia are also required for COC pickup, and this function may be dependent upon proper

adhesion between COC matrix and cilia crown. In addition to COC pickup, adhesive interactions between sperm and oviductal cilia and the roles of these interactions in regulating sperm storage and migration have been reported in several species (21, 22). Therefore, normal structure and function of motile cilia appear to be required for the normal adhesive interactions between oviductal epithelium and gametes as well as preimplantation embryos. Indeed, a lack of motile cilia in the oviductal epithelium abolishes the COC pickup function completely, whereas the sperm and embryo transport function is only partially compromised. Together, the function of motile cilia in both COC pickup and sperm migration may be mainly attributed to adhesive interactions, which warrant further investigations in the future.

The finding that functional motile cilia in the infundibulum are required for COC pickup during ovulation and the subsequent transport to the ampulla of the oviducts has important clinical implications. First, infertility of the female mice lacking the two miRNA clusters results from defects in motile cilia because infundibulum of the oviducts cannot pick up and transport the ovulated COCs to the ampulla region. If a similar situation exists in women, the most likely diagnosis would be idiopathic infertility because these patients would have no tubal obstructions and display normal hormonal profiles and normal ovarian functions. However, these women may have defective motile cilia, leading to a failure in COC pickup and transport. Second, if factors that can induce motile cilia dysfunction or inhibit differentiation of the oviductal precursor cells into ciliated cells, for example, inflammation, environmental toxins, chemotherapy, allergy, etc., can be identified, treatment for female idiopathic infertility caused by motile ciliopathy would become feasible. Third, the absolute requirement of functional motile cilia in the infundibulum for COC capture and, thus, female fertility suggests that inhibition of oviductal motile cilia may represent an ideal means to develop female nonhormonal contraceptives. If an agent can specifically inhibit replenishment and/or motility of the oviductal, but not other, motile cilia, then the ovulated oocytes would be lost, thus achieving contraception.

The relative contribution of smooth muscle contraction and cilia beating to sperm transport from the isthmus to the ampulla and migration of the preimplantation embryos from the ampulla to the uterine cavity has been debated for a long time. The notion that motile cilia represent the major force driving sperm and embryo transport was based on earlier reports showing that by inhibiting smooth muscle contraction using isoproterenol, the transport function of the oviduct appeared to be normal (3, 4). However, these studies utilized surrogate microspheres to imitate oocytes and albumin to imitate the cumulus. These surrogate microspheres used were much smaller (15 μm in diameter) than the native oocytes within the naturally ovulated COCs (70 to 90 μm in diameter). Moreover, isoproterenol is known to also increase ciliary beating, which may have amplified the effects of ciliary beating (3, 4). The opposing view supporting smooth muscle contraction, not motile cilia beating, as the major force driving sperm and embryo transport is based on several studies (14) (5–8, 23). Blocking smooth muscle contractions with the L-type Ca^{2+} channel antagonist nicardipine caused oviduct stasis and inhibited egg movements. Nicardipine did not affect ciliary beating, as assessed by the movement of particles along the luminal surface of the duct (14). Some mutant mice with ciliary dyskinesia can produce pups through natural mating, and some women with Kartagener's syndrome gave birth to children following spontaneous conception (5–8, 23). Despite largely normal smooth muscle functions, the KO oviductal epithelium either completely lacks or contains a much reduced number of structurally defective motile cilia, thus allowing us to define the relative contribution of ciliate beating to the sperm and early embryo transport function of the oviducts. The fact that WT sperm still manage to reach the ampulla region of the miR-dKO oviducts despite reduced efficiency and ∼50% of the early embryos transferred to the ampulla region of the miR-dKO oviducts also successfully migrate to the uterus for implantation strongly indicates that motile cilia beating facilitates the transport function, but it is not absolutely required for sperm and embryo transport in the oviducts in mice.

It remains puzzling why among women with primary ciliary dyskinesia (PCD), some are fertile or subfertile, whereas others are completely infertile (24). Based on literature and our data reported here, we believe that the following factors affect the fertility outcome in women with PCD. First is the severity of motile cilia defects as reflected by the number of multiciliated cells, the number of cilia on each ciliated cell, and the motility of the cilia. Because these three aspects can be genetically controlled by three separate pathways, the phenotypic severity can be highly variable depending upon the genes that are implicated in the patients. For example, if a mutation occurs in a gene responsible for replenishment of ciliated cells by oviductal epithelial stem cells, the number of total ciliated cells may decrease over time despite the normal number of cilia on each ciliated cell and normal motility of the cilia; consequently, the patient may be fertile at a younger age but become infertile with aging. Similarly, if a mutation occurs in a gene essential for cilia elongation, then both the number of ciliated cells and the number of cilia per cell may be normal, but the motility is abnormal due to shorter cilia. In our conditional KO females, 30% of the conditional females are initially fertile and gradually become infertile after 6 wk of age. This is because deletion of the two miRNA gene clusters only takes place after *Foxj1* starts to be expressed ∼P4. However, at P4, ciliated cells have started their differentiation and cilia have started to form. Consequently, normal oviductal epithelia are present in these conditional KO females initially. However, persistent absence of the two miRNA gene clusters disrupts the subsequent multiciliogenesis; that is, the newly formed ciliated cells and their cilia are both compromised, leading to increased severity in cilia dysfunction and progressive loss of female fertility. Second, although multiciliogenesis may be largely conserved, the motile cilia in the trachea, oviducts, efferent ducts, and brain are clearly different in their length, density, beating pattern, and frequency, suggesting the existence of some tissue-specific genetic networks (25–27). If the mutations occur in these tissue-specific genes, then the patient may have motile cilia defects only in one or two of these multiciliated organs. Therefore, one cannot assume that all of the multiciliated organs are equally affected in patients with PCD. It is possible that a woman with PCD may have severe defects on tracheal motile cilia but very minor or even normal motile cilia in their oviducts. Third, other anatomical and physiological differences between mice and humans may also contribute to the variable infertility phenotype in women with PCD. However, the detailed process of COC pickup is much less understood in humans than in mice. Although many factors, including bursa-like structure in humans (e.g., the pouch of Douglas), smooth muscle contraction ("sucking" effect), adhesion between COCs and oviductal epithelia, ciliary beating, etc., have been proposed to contribute to COC pickup, our data reported here strongly suggest that a normal number of ciliated cells and normal ciliary beating are absolutely required for COC pickup. It is of great interest to further define whether the ciliated cells function to adhere (COC-cilia adhesion) or transport (moving COC from bursa to the ostium), or both.

In summary, our data support the notion that normal motile cilia in the infundibulum are essential for oocyte pickup and transport, and motile cilia in the ampulla and isthmus regions of the oviducts facilitate gamete and embryo transport but are not absolutely required for female fertility.

Materials and Methods

Animals. All animal work was performed following the protocol approved by the Institutional Animal Care and Use Committee of the University of Nevada,

Reno. Mice were housed and maintained under specific pathogen-free conditions with a temperature- and humidity-controlled animal facility in the University of Nevada, Reno. The *miR-449* and *miR-34b/c* miR-dKO mice were generated as described (9, 28). The miR-449 loxP mouse line was generated as described (16). The *Stra8-Cre*, *Foxj1-Cre*, and *Rosa26-mTmG* mice were purchased from The Jackson Laboratory. *Stra8-Cre-mTmG*$^{+/Tg}$ mice were generated as described (29). All mice used in this study were on the C57BL/6J background. WT and *miR-dKO* oviducts used in this study were collected from the mice which underwent superovulation by injection of 5 international unit (IU) pregnant mare's serum gonadotropin followed by 5 IU human chorionic gonadotropin (hCG) injection 48h later.

Histology and Immunofluorescence. For histology, tissues were dissected under a dissection microscope and fixed in Bouin's solution overnight at 4 °C followed by dehydration and paraffin embedding. Paraffin sections (4 μm) were cut using a microtome and stained with the hematoxylin and eosin after deparaffinization and rehydration. For immunofluorescent staining, tissue samples were fixed in 4% paraformaldehyde in phosphate-buffered saline (PBS) overnight at 4 °C and then embedded in 20% sucrose and optimal cutting temperature (OCT) compound (1:1) (Tissue-Tek, no. 4583). Cryosections (5 μm) were cut at −20 °C, and the sections were washed twice in PBS with 0.05% Tween 20. After blocking in PBSTB (0.1% Triton X-100, 1% bovine serum albumin in PBS) at room temperature for 1 h, the slides were incubated with primary antibodies at 4 °C overnight. The primary antibodies used included anti–β-tubulin IV monoclonal antibody (TUBB4, 1:20; BioGenex, MU178-UC), anti–acetylated-α-tubulin (1:500; Sigma T6793), and anti-PAX8 (1:200; ProteinTech Group, Inc.). After washing three times with cold PBST (0.1% Triton X-100 in PBS), the slides were incubated with a secondary antibody (1:1,000, Alexa Fluor 488 goat anti-rabbit, Molecular Probes A-11034 or Alexa Fluor 555 conjugate goat anti-mouse, Molecular Probes A-21422) at room temperature for 1 h. Slides were then mounted with VECTASHIELD mounting medium containing DAPI (Vector Laboratories, no. H-1200). Images were taken with an epifluorescence microscope (Axioplan 2, Carl Zeiss).

Cell Counting. To determine the relative density of ciliated and secretory cells, dual color immunofluorescent staining using beta-Tubulin IV (ciliated cells) and PAX8 (secretory) antibodies was conducted. Green and red cells were counted separately using the corresponding filter set under an epifluorescence microscope (Axioplan 2, Carl Zeiss). A minimum of 400 epithelial cells per section were counted, and a total of 10 to 20 sections were analyzed. Student's *t* test was employed for statistical analyses, and $P < 0.05$ was regarded as statistically significant.

TEM. TEM was performed as described previously with some modifications (30). Briefly, the oviducts were fixed in 0.1 M cacodylate buffer (pH 7.4) containing 3% paraformaldehyde and 3% glutaraldehyde plus 0.2% picric acid for 2 h in 4 °C, then for 1 h at RT. Following washes with 0.1 M cacodylate buffer, the samples were postfixed with 1% OsO4 for 1 h at RT. The samples were then dehydrated followed by embedding in Eponate mixture (Electron Microscopy Sciences) for polymerization for ∼24 h at 60 °C. Ultrathin sections (60 to 70 nm) were cut with a diamond knife. The sections were stained with uranyl acetate and lead citrate and then photographed using a TEM (Phillips CM10) at 80 kV.

Separation of Oviductal Epithelium and Smooth Muscle. To obtain enriched oviductal epithelial and smooth muscle cells, we adopted a previously reported method (31) with slight modifications to separate oviductal epithelium from the smooth muscle layers. In brief, the oviducts were dissected from adult WT and miR-dKO female mice and then transferred to 1× Hanks' balanced salt solution (HBSS) solution (HyClone, GE Healthcare, catalog no. SH3058801) containing 1% trypsin (catalog no. T-4799, Sigma), followed by incubation at 4 °C for 90 min and then at 22 °C for 30 min. After incubation, the oviducts were rinsed in 20% fetal bovine serum in 1× HBSS solution (HyClone, no. SH30588) and then treated with 0.1% deoxyribonuclease 1 (catalog no. DN25, Sigma) in 1× HBSS. Epithelial and smooth muscle layers were separated by gentle suction of the oviducts through a glass capillary pipette under a stereomicroscope. The separated epithelial and smooth muscle layers were washed several times with PBS and then transferred into 1.5-mL Eppendorf tubes for RNA extraction or onto a glass slide for morphological observation.

qPCR Analysis. RNA (large and small) was isolated from the oviducts of WT and miR-dKO mice using the mirVana miRNA isolation kit (Ambion, catalog no. AM1560). Large RNAs were reverse transcribed to complementary DNAs (cDNAs), which were then diluted to 50 ng/μL and used for qPCR analyses using FAST SYBR Green (Applied Biosystems). For miRNA qPCR analyses, we performed them as described (9, 28). qPCR analyses were performed on 7900HT Fast Real-Time PCR System (Applied Biosystems). Relative quantification was performed with *Gapdh* serving as the endogenous control, and expression levels were further normalized against WT samples. U6 small nuclear RNA was used as miRNA qPCR data normalization. Data were analyzed by Student's *t* test. A statistically significant difference was defined as $P < 0.05$. The primer sequences are listed in *SI Appendix*, Table S4.

Sperm Migration Analysis. *Stra8-Cre-mTmG*$^{+/Tg}$ males were introduced into the cages of superovulated WT and miR-dKO females ∼12 h after hCG injection, and the females were checked for the presence of vaginal plugs every 30 min. At ∼2 h after copulation (the sight of plugs), the oviducts were separated from the uterine horns and straightened out by cutting the mesosalpinx under a stereo microscope. Then the oviducts were transferred onto slides as whole mounts, covered with coverslips supported by pillars of paraffin: petroleum jelly (1:10), and examined using a green fluorescence filter set to identify the sperm inside the oviducts under a microscope with epifluorescence.

Embryo Transfer Assay. To study the embryo transport, two-cell stage WT embryos (10–15) were transferred into the oviducts of WT and *miR-dKO* pseudopregnant females 0.5 d after mating with vasectomized males. For uterus transfer, WT blastocysts (10–15) were transferred into the uterus of WT and *miR-dKO* pseudopregnant females 2.5 d after mating with vasectomized males. The presence of vaginal plugs was designated as postcoitum day 0.5, and pups were born on day 19 for oviductal transfer and on day 17 for uterus transfer.

Imaging Analyses of Ciliary Beating. Oviducts were cut into small (∼1 mm) pieces in HBSS solution (HyClone, no. SH30588) under a dissection microscope and then transferred to a glass slide as whole mounts and covered with a coverslip supported by pillars of paraffin: petroleum jelly (1:10). Movies of cilial movement were captured using a high-speed camera (Imagingsource, DMK 21AF04n) attached to a microscope (Carl Zeiss, Axioskop 2) at 240 frames per second. Quantitative imaging analyses of cilia movement were performed as described previously (15).

Oviductal Smooth Muscle Intracellular Recording. The female reproductive tracts were removed from WT and miR-dKO mice via an abdominal incision immediately following cervical dislocation and placed in Krebs-Ringer bicarbonate solution (KRB). Oviducts were dissected free from the ovary and uterine horn and uncoiled by sharp dissection to yield single intact oviduct preparations comprising the ampulla, isthmus, and intramural segments. Tissues were perfused with KRB containing the following (mmol/L): NaCl, 120.35; KCl, 5.9; $NaHCO_3$, 15.5; NaH_2PO_4, 1.2; $MgCl_2$, 1.2; $CaCl_2$, 2.5; and glucose, 11.5. KRB was bubbled with a mixture of 97% O_2 and 3% CO_2 and warmed to a physiologically relevant temperature of 37 ± 0.5 °C. In these conditions, the pH of the KRB was maintained between 7.3 to 7.4. Intact uncoiled oviduct preparations were pinned to the base of a Sylgard-elastomer (Dow Corning)–lined recording chamber using fine tungsten pins (50-μm diameter) to restrict movement of the muscle and extend the length of time, and impalement could be maintained. Tissues were allowed to equilibrate for at least 1 h prior to the commencement of experiments. After this time, individual smooth muscle cells within the myosalpinx of the ampulla and isthmus regions were impaled using sharp glass microelectrodes, which had resistances of 80 to 120 MΩ, and were filled with 3 M KCl. The potential difference across the smooth muscle cell membrane was recorded using a high impedance electrometer (Axoclamp 2B, Axon Instruments/Molecular Devices). These data were digitized using a Digidata 1322A (Axon Instruments) and recorded onto a PC using Axoscope 10.1 (Axon Instruments) software. Final figures were prepared from digitized data using Corel Draw 14.0 (Corel Corp.).

RNA-seq and Data Analysis. Large RNAs were isolated from the WT and miR-dKO oviducts using the AquaRNA RNA Purification Kit (catalog no. 5001MT, MoBiTec, Inc.). The mRNA libraries were constructed using the TruSeq Stranded Total RNA Library Prep Kit (catalog no. RS-122-2201, Illumina). Sequencing was conducted using Hi-SEq. 4000 sequencers with PE75 at the BGI bioscience. The FASTX-Toolkit was used to remove adaptor sequences and low-quality reads from the sequencing data. To identify all the transcripts, we used Tophat2 and Cufflinks to assemble the sequencing reads based on the University of California, Santa Cruz (UCSC) MM9 mouse genome (32). The differential expression analyses were performed by Cuffdiff (32). The global statistics and quality controls are presented in *SI Appendix*, Fig. S8. The untranslated region (UTR) and alternative splicing analyses were

performed using the SpliceR pipeline (33). R script was used to assist the data mining.

In Silico miRNA Target Prediction. The 3′ UTR sequence for each mRNA isoform was extracted using in-house R script based on ref. 33. RNAhybrid was used to perform the binding analyses between the 3′ UTR sequence and the miRNA sequence (RNAhybrid –c –s 3utr_human –p 0.1-f 2,7) as described previously (34). The output results were imported into R as data frame for downstream analyses.

Luciferase Reporter Assay. For luciferase reporter assays, the 3′ UTR of *Tubb4b* was synthesized by Integrated DNA Technologies (IDT) and amplified by PCR using GoTaq Green Master Mix (M7123, Promega). After being digested with Xho I (R0146S, NEB) and Not I (R3189S, NEB) restriction enzymes, the PCR products were inserted into the psiCHECK-2 vector (C8021, Promega) at the downstream of the Renilla luciferase-coding sequence. HEK293 cells were cotransfected with 5 pmol miRNA mimics or NC (GE Dharmacon) and 150 ng psiCHECK-2 containing the *Tubb4b*-3′ UTR using Lipofectamine 2000 (11668, Invitrogen) in a 24-well cell culture plate (3524, Corning). After 24 h of culture, cells were lysed and assayed with Dual Luciferase Assays (E1910, Promega) according to the manufacturer's instructions. Renilla luciferase signals were normalized to Firefly luciferase signal to qualify the transfection efficiency. The primers were synthesized by IDT, and the sequences are as follows (underlined are Xho I and Not I restriction sites, respectively): *Tubb4b* 3′ UTR Forward: CATCTCGAGGAGCTGTCTTAGTCACTAAAGCATG; *Tubb4b* 3′ UTR Reverse: GATGCGGCCGCGCCACACACTATGAATTGCTT.

Statistical Analysis. All data were shown as mean ± SEM, and statistical differences between datasets were assessed by one-way ANOVA or *t* test using the SPSS16.0 software. $P < 0.05$ was considered as significant differences, and $P < 0.01$ was considered as highly significant differences. Embryo transfer data were analyzed using X^2 tests, and $P < 0.05$ was regarded as significant differences.

Data Availability. The RNA-seq data have been deposited into the National Center for Biotechnology Information Sequence Read Achieve database (accession no. PRJNA464042) (35).

ACKNOWLEDGMENTS. We would like to thank Dr. Michael Kessel, Max Planck Institute for Biophysical Chemistry, Germany, for generously providing us with the cryopreserved embryos for rederivation of the miR-449-loxp mouse line. This work was supported, in part, by grants from the NIH (HD071736, HD0085506, HD098593, and HD099924 to W.Y.) and the Templeton Foundation (Project ID: 61174 to W.Y.).

1. C. A. Stewart, R. R. Behringer, "Mouse oviduct development" in *Mouse Development*, J. Z. Kubiak, Ed. (Springer-Verlag, Berlin, Heidelberg, 2012), chap. 14, pp. 247–262.
2. P. Coy, F. A. García-Vázquez, P. E. Visconti, M. Avilés, Roles of the oviduct in mammalian fertilization. *Reproduction* **144**, 649–660 (2012).
3. S. A. Halbert, D. R. Becker, S. E. Szal, Ovum transport in the rat oviductal ampulla in the absence of muscle contractility. *Biol. Reprod.* **40**, 1131–1136 (1989).
4. S. A. Halbert, P. Y. Tam, R. J. Blandau, Egg transport in the rabbit oviduct: The roles of cilia and muscle. *Science* **191**, 1052–1053 (1976).
5. K. Baker, P. L. Beales, Making sense of cilia in disease: The human ciliopathies. *Am. J. Med. Genet. C. Semin. Med. Genet.* **151C**, 281–295 (2009).
6. R. A. Lyons, E. Saridogan, O. Djahanbakhch, The reproductive significance of human Fallopian tube cilia. *Hum. Reprod. Update* **12**, 363–372 (2006).
7. H. B. Croxatto, Physiology of gamete and embryo transport through the fallopian tube. *Reprod. Biomed. Online* **4**, 160–169 (2002).
8. J. R. Blake, Mechanics of ciliary transport. *Prog. Clin. Biol. Res.* **80**, 41–45 (1982).
9. J. Wu *et al*., Two miRNA clusters, miR-34b/c and miR-449, are essential for normal brain development, motile ciliogenesis, and spermatogenesis. *Proc. Natl. Acad. Sci. U.S.A.* **111**, E2851–E2857 (2014).
10. Y. Zhang *et al*., A transgenic FOXJ1-Cre system for gene inactivation in ciliated epithelial cells. *Am. J. Respir. Cell Mol. Biol.* **36**, 515–519 (2007).
11. A. Ghosh, S. M. Syed, P. S. Tanwar, *In vivo* genetic cell lineage tracing reveals that oviductal secretory cells self-renew and give rise to ciliated cells. *Development* **144**, 3031–3041 (2017).
12. M. Ezzati, O. Djahanbakhch, S. Arian, B. R. Carr, Tubal transport of gametes and embryos: A review of physiology and pathophysiology. *J. Assist. Reprod. Genet.* **31**, 1337–1347 (2014).
13. R. Dixon, S. Hwang, F. Britton, K. Sanders, S. Ward, Inhibitory effect of caffeine on pacemaker activity in the oviduct is mediated by cAMP-regulated conductances. *Br. J. Pharmacol.* **163**, 745–754 (2011).
14. R. E. Dixon *et al*., Chlamydia infection causes loss of pacemaker cells and inhibits oocyte transport in the mouse oviduct. *Biol. Reprod.* **80**, 665–673 (2009).
15. S. Yuan *et al*., Motile cilia of the male reproductive system require miR-34/miR-449 for development and function to generate luminal turbulence. *Proc. Natl. Acad. Sci. U.S.A.* **116**, 3584–3593 (2019).
16. R. Song *et al*., miR-34/449 miRNAs are required for motile ciliogenesis by repressing cp110. *Nature* **510**, 115–120 (2014).
17. P. Talbot, B. D. Shur, D. G. Myles, Cell adhesion and fertilization: Steps in oocyte transport, sperm-zona pellucida interactions, and sperm-egg fusion. *Biol. Reprod.* **68**, 1–9 (2003).
18. X. Lam, C. Gieseke, M. Knoll, P. Talbot, Assay and importance of adhesive interaction between hamster (Mesocricetus auratus) oocyte-cumulus complexes and the oviductal epithelium. *Biol. Reprod.* **62**, 579–588 (2000).
19. J. T. Norwood, C. E. Hein, S. A. Halbert, R. G. Anderson, Polycationic macromolecules inhibit cilia-mediated ovum transport in the rabbit oviduct. *Proc. Natl. Acad. Sci. U.S.A.* **75**, 4413–4416 (1978).
20. P. Talbot, C. Geiske, M. Knoll, Oocyte pickup by the mammalian oviduct. *Mol. Biol. Cell* **10**, 5–8 (1999).
21. S. S. Suarez, A. A. Pacey, Sperm transport in the female reproductive tract. *Hum. Reprod. Update* **12**, 23–37 (2006).
22. S. S. Suarez, Mammalian sperm interactions with the female reproductive tract. *Cell Tissue Res.* **363**, 185–194 (2016).
23. J. Raidt *et al*., Ciliary function and motor protein composition of human fallopian tubes. *Hum. Reprod.* **30**, 2871–2880 (2015).
24. K. Praveen, E. E. Davis, N. Katsanis, Unique among ciliopathies: Primary ciliary dyskinesia, a motile cilia disorder. *F1000Prime Rep.* **7**, 36 (2015).
25. M. Legendre, L. E. Zaragosi, H. M. Mitchison, Motile cilia and airway disease. *Semin. Cell Dev. Biol.* **110**, 19–33 (2021).
26. L. Lee, L. E. Ostrowski, Motile cilia genetics and cell biology: Big results from little mice. *Cell. Mol. Life Sci.* **78**, 769–797 (2021).
27. C. Ringers, E. W. Olstad, N. Jurisch-Yaksi, The role of motile cilia in the development and physiology of the nervous system. *Philos. Trans. R. Soc. Lond. B Biol. Sci.* **375**, 20190156 (2020).
28. S. Yuan *et al*., mir-34b/c and mir-449a/b/c are required for spermatogenesis, but not for the first cleavage division in mice. *Biol. Open* **4**, 212–223 (2015).
29. Q. Wu *et al*., The RNase III enzyme DROSHA is essential for microRNA production and spermatogenesis. *J. Biol. Chem.* **287**, 25173–25190 (2012).
30. S. Yuan, H. Zheng, Z. Zheng, W. Yan, Proteomic analyses reveal a role of cytoplasmic droplets as an energy source during epididymal sperm maturation. *PLoS One* **8**, e77466 (2013).
31. H. Yamanouchi, T. Umezu, Y. Tomooka, Reconstruction of oviduct and demonstration of epithelial fate determination in mice. *Biol. Reprod.* **82**, 528–533 (2010).
32. C. Trapnell *et al*., Differential gene and transcript expression analysis of RNA-seq experiments with TopHat and Cufflinks. *Nat. Protoc.* **7**, 562–578 (2012).
33. K. Vitting-Seerup, B. T. Porse, A. Sandelin, J. Waage, spliceR: An R package for classification of alternative splicing and prediction of coding potential from RNA-seq data. *BMC Bioinformatics* **15**, 81 (2014).
34. J. Krüger, M. Rehmsmeier, RNAhybrid: microRNA target prediction easy, fast and flexible. *Nucleic Acids Res.* **34**, W451–W454 (2006).
35. S. Yuan, W. Yan, Mus musculus strain:C57 (house mouse). The National Center for Biotechnology Information BioProject. https://www.ncbi.nlm.nih.gov/bioproject/PRJNA464042. Deposited 4 May 2018.

PHYSIOLOGY